

Aptamer-Functionalized Bioscaffold Enhances Cartilage Repair by Improving Stem Cell Recruitment in Osteochondral Defects of Rabbit Knees

Xin Wang,^{*} MSc, Xiongbo Song,^{*} MS, Tao Li,^{*} MSc, Jiajia Chen,[†] BSc, Guotao Cheng,[†] MSc, Liu Yang,^{*§} MD, PhD, and Cheng Chen,^{*§} PhD

Investigation performed at Center for Joint Surgery, Southwest Hospital, Third Military Medical University, Chongqing, China

Background: Recruitment of endogenous stem cells has been considered an alternative to cell injection/implantation in articular cartilage repair.

Purpose: (1) To develop a cartilage tissue-engineering scaffold with clinically available biomaterials and functionalize the scaffold with an aptamer (Apt19s) that specifically recognizes pluripotent stem cells. (2) To determine whether this scaffold could recruit joint-resident mesenchymal stem cells (MSCs) when implanted into an osteochondral defect in a rabbit model and to examine the effects of cartilage regeneration.

Study Design: Controlled laboratory study.

Methods: The reinforced scaffold was fabricated by embedding a silk fibroin sponge into silk fibroin/hyaluronic acid-tyramine hydrogel and characterized in vitro. A cylindrical osteochondral defect (3.2 mm wide × 4 mm deep) was created in the trochlear grooves of rabbit knees. The rabbits were randomly assigned into 3 groups: Apt19s-functionalized scaffold group, scaffold-only group, and control group. Animals were sacrificed at 6 and 12 weeks after transplantation. Repaired tissues were evaluated via gross examination, histologic examination, and immunohistochemistry.

Results: In vitro, this aptamer-functionalized scaffold could recruit bone marrow-derived MSCs and support cell adhesion. In vivo, the aptamer-functionalized scaffold enhanced cell homing in comparison with the aptamer-free scaffold. The aptamer-functionalized scaffold group also exhibited superior cartilage restoration when compared with the scaffold-only group and the control group.

Conclusion: The Apt19s-functionalized scaffold exhibited the ability to recruit MSCs both in vitro and in vivo and achieved a better outcome of cartilage repair than the scaffold only or control in an osteochondral defect model.

Clinical Relevance: The findings demonstrate a promising strategy of using aptamer-functionalized bioscaffolds for restoration of chondral/osteochondral defects via aptamer-introduced homing of MSCs.

Keywords: cartilage repair; aptamer; mesenchymal stem cells; osteochondral defect

Articular cartilage has very low cellularity and no blood supply; moreover, it is subjected to continuous mechanical loading.³⁸ The unique nature of cartilage plus the complex environment in which it resides makes the repair of an articular cartilage defect an enormous challenge. To date, none of the clinical treatments are able to fully restore injured articular cartilage.³¹ One critical problem in cartilage repair is the cell source. Autologous chondrocytes and mesenchymal stem cells (MSCs) are the most widely used

cells in cell-based cartilage repair and cartilage tissue engineering.^{4,29} However, during the repair process, such as autologous chondrocyte implantation, chondrocytes need in vitro expansion, which usually results in the dedifferentiation of chondrocytes and the eventual formation of fibrous cartilage.^{27,35} MSCs from other tissues (bone marrow, fat, etc) tend to undergo hypertrophic differentiation, which finally results in calcification.^{32,34} In this case, cartilage repair by recruiting endogenous stem cells in situ has been given much attention.^{11,19}

Although MSCs are rare in cartilage tissue, they are abundant in the other joint tissues (ie, subchondral bone, synovial fluid, synovium, and adipose tissue).^{2,5,30} Therefore, it is theoretically possible to recruit the MSCs nearby

to migrate to the cartilage defects. As a matter of fact, one of the clinical treatments, microfracture,¹ utilizes MSCs from the bone marrow to migrate toward the injury site and help repair cartilage. However, the long-term clinical outcome of microfracture is usually less than satisfactory.^{36,37} The main reasons include the following: (1) during the repair process, there is no scaffolding material in the site such that the MSCs/neocartilage are directly exposed to continuous compressive loading and shear forces¹⁴; (2) the number of the MSCs spontaneously migrating toward the cartilage defect might be insufficient to regenerate cartilage of a such volume.¹³ These problems could be solved by implanting a biomechanically compatible scaffold capable of recruiting MSCs *in situ*.

Silk fibroin (SF), a natural biopolymer extracted from *Bombyx mori* cocoons, has been widely used in cartilage tissue engineering, owing to its good biocompatibility and excellent mechanical strength.^{12,41,43} To improve the chondrogenic capacity of SF-based hydrogels, hyaluronic acid (HA) can be incorporated since it has been shown to promote chondrogenesis both *in vitro* and *in vivo*.^{7,21,40} Aptamers are short stretches of nucleotides or amino acid residues, which can bind to specific targets, such as small chemical groups, large proteins, and even live cells.⁴⁸ Recently, an aptamer named Apt19s was reported to label human pluripotent stem cells.¹⁶ In this study, we first prepared a SF/HA composite hydrogel. Then, this hydrogel was enhanced by embedding a mechanically robust SF sponge that was earlier functionalized with Apt19s. In this way, a reinforced hydrogel sponge scaffold was fabricated with the possible capacity of recruiting pluripotent stem cells. Finally, the morphology, mechanical properties, swelling behaviors, degradation, and MSC recruitment ability of the hydrogel sponge scaffold were studied *in vitro*. The outcome of cartilage defect repair was tested by implanting the hydrogel sponge scaffold into a rabbit osteochondral defect model (Figure 1A).

METHODS

In Vitro Studies

Preparation of Aptamer-Functionalized SF Sponge. *B. mori* cocoons were kindly provided by the Institute of Biotechnology of Southwest University. SF solution was prepared as described in our previous publication.²⁵ For the fabrication of SF sponges, SF solution (60 mg/mL) in a cylinder mold (diameter, 6 mm; height, 10 mm) was sequentially

frozen at -20°C for 6 hours and at -80°C overnight. Then, the SF sponges were freeze-dried, immersed in 75% ethanol for 30 minutes to achieve β-sheet formation, and finally cut by a custom-made hole puncher (1.5 mm, 2 mm, 5 mm) for the following experiments.

The binding of aptamer (amino-modified Apt19s: 5'-NH₂-[A]9-AGGTTCAGATGAGGAGGGACTTAGGACTGGGTTTATGACCTATGCGTG-3', synthesized by Sangon Biotech) to SF sponge was performed according to a recent protocol.¹⁷ Briefly, an SF sponge was immersed in 2 mL of morpholinoethanesulfonic acid (0.1 M, pH = 6; Macklin). The carboxyl groups of SF were activated by adding 8 mg of EDC (1-ethyl-3-[3-dimethylaminopropyl] carbodiimide hydrochloride; J&K) and 12 mg of NHS (N-hydroxysuccinimide; J&K) for 15 minutes at room temperature. Then the activation buffer was removed, and the SF sponge was washed twice with phosphate buffer solution (PBS). For the conjugation of aptamer, 4 nmol of amino-modified Apt19s in 2 mL of PBS was added and reacted for 12 hours in a reciprocating oscillator. The aptamer-functionalized SF sponge was washed twice with PBS.

Preparation of SF/HA-Tyramine Hydrogel. HA-tyramine (Tyr) conjugates were prepared according to an established procedure.²⁴ The degree of substitution of Tyr (J&K) residues in HA-Tyr conjugates, defined as the number of Tyr moieties per 100 repeating units of HA, was determined by ¹H nuclear magnetic resonance.

SF/HA-Tyr hydrogels were prepared by enzymatically crosslinking. Briefly, HA-Tyr conjugates were dissolved in 30 mg/mL of SF solution to yield a final HA-Tyr concentration of 0% (pure SF), 10%, 15%, 20%, or 100% (10 mg/mL of HA-Tyr in deionized water without SF). Ten microliters of horseradish peroxidase solution (1000 U/mL) was added to 1 mL of SF/HA-Tyr solution; then, 10 μL of H₂O₂ (1% v/v) was added and mixed by gentle pipetting. The gelation time was recorded with the vial tilting method. No flow within 1 minute upon inverting the vial was regarded as the gel state.

Fabrication of the Sponge/Hydrogel Scaffold. For the reinforced sponge/hydrogel scaffold, SF sponges were immersed in SF/HA-Tyr solutions in a custom-made cylinder mold (3.2 mm or 10 mm) overnight to enable replete infiltration; then, horseradish peroxidase and H₂O₂ were added as the preparation of SF/HA-Tyr hydrogel mentioned earlier.

Morphology. The scaffolds were freeze-dried, crosscut, and sputter-coated with gold. The morphologies of the section were viewed with a ZEISS Crossbeam 340 scanning electron microscope (SEM) operated at 2-kV accelerating voltage.

[§]Address correspondence to Liu Yang, MD, PhD, Center for Joint Surgery, Southwest Hospital, Third Military Medical University, Chongqing 400038, China (email: jointsurgery@163.com); Cheng Chen, PhD, Center for Joint Surgery, Southwest Hospital, Third Military Medical University, 30 Gaotanyan Street, Chongqing 400038, China (email: cclijff@163.com).

^{*}Center for Joint Surgery, Southwest Hospital, Third Military Medical University, Chongqing, China.

[†]Biomedical Analysis Center, Third Military Medical University, Chongqing, China.

[‡]College of Biotechnology, Southwest University, Chongqing, China.

X.W. and X.S. contributed equally to this article.

One or more of the authors has declared the following potential conflict of interest or source of funding: This study was supported by National Natural Science Foundation of China grant 81572107 to L.Y. AOSSM checks author disclosures against the Open Payments Database (OPD). AOSSM has not conducted an independent investigation on the OPD and disclaims any liability or responsibility relating thereto.

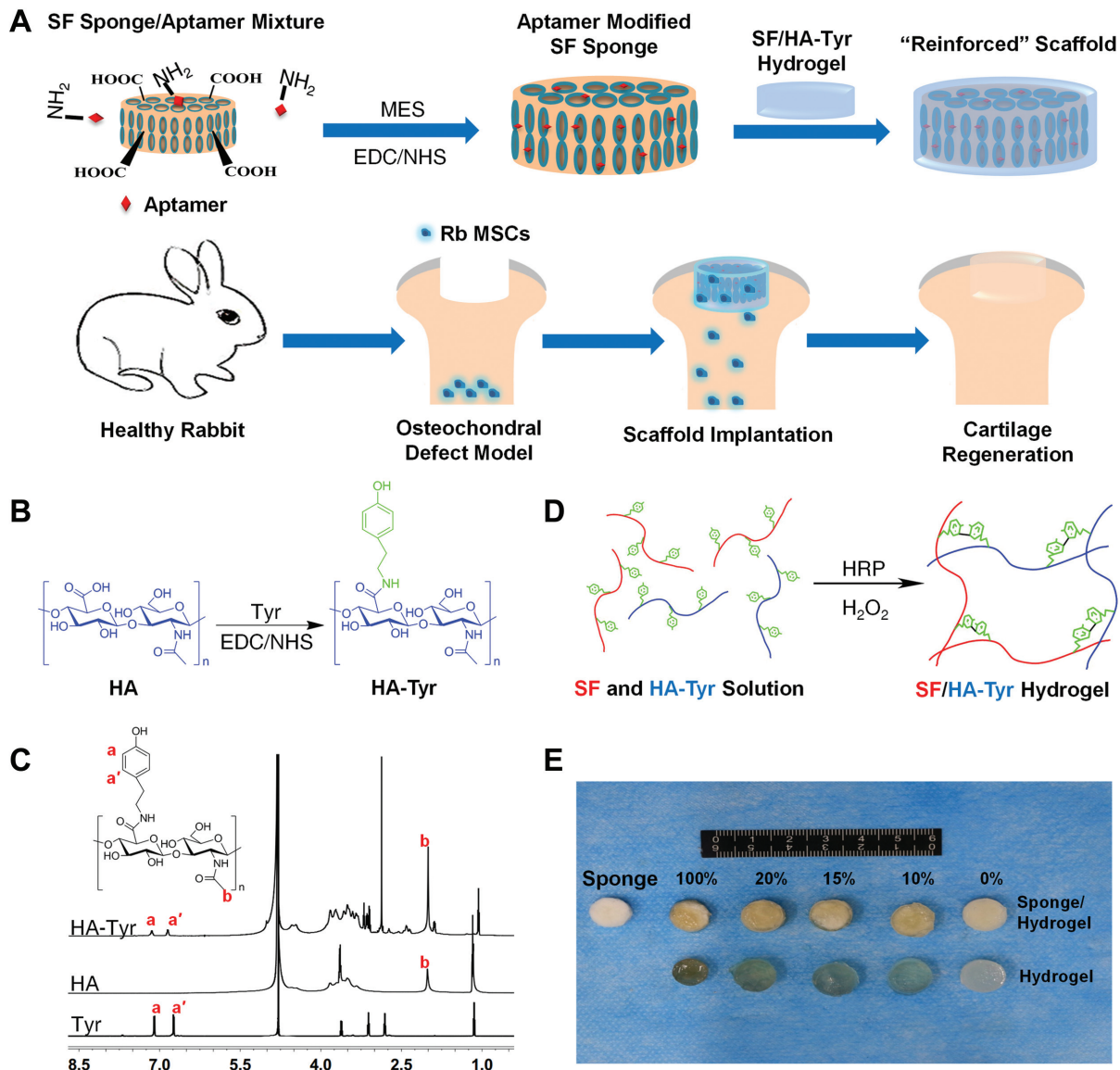


Figure 1. Study design and experimental scheme for the aptamer-functionalized reinforced sponge/hydrogel scaffold. (A) Schematic diagram. (B) Preparation of hyaluronic acid (HA) and tyramine (Tyr) conjugates. (C) Conjugation of HA and Tyr was confirmed by ^1H nuclear magnetic resonance. (D) Gelation mechanism of silk fibroin (SF) / HA-Tyr hydrogel. (E) Macroscopic appearance of SF sponge, HA-Tyr hydrogel, and sponge/hydrogel scaffold. EDC, 1-ethyl-3-[3-dimethylaminopropyl] carbodiimide hydrochloride; HRP, horseradish peroxidase; MES, morpholinoethanesulfonic acid; NHS, N-hydroxysuccinimide; Rb MSCs, rabbit mesenchymal stem cells.

Equilibrium Swelling. The freeze-dried scaffolds (weighed as W_1) were immersed in PBS at 37°C for 2 days until equilibrium of swelling was reached. The weight of fully swollen scaffolds was recorded immediately after the excess of water lying on the surfaces was absorbed with filter paper (weighed as W_2). The equilibrium swelling ratio was calculated with the following equation: $(W_2 - W_1) / W_2 \times 100\%$.

Degradation In Vitro. Degradation of scaffolds was carried out in PBS at 37°C for 4 weeks or in type XIV protease (Sigma-Aldrich) solution at 37°C for 1 week. The initial weight of dry samples was determined (W_1). At specified

time intervals, the samples were dehydrated and weighed (W_2). The weight-remaining ratio was defined as $(W_1 - W_2) / W_1 \times 100\%$.

Mechanical Testing. The compressive modulus of the scaffolds with known size was measured with an Instron 5969 testing frame (Instron Instruments) with a prestrain force of 0.1 N and constant compression speed of 1.5 mm/min till rupture or 100% strain. The compressive modulus was obtained from the linear elastic region of the stress-strain curve (30% and 40% strain).

Isolation and Culture of Rabbit Bone Marrow-Derived MSCs. Rabbit bone marrow-derived MSCs (BMSCs) were

harvested from 3-month-old New Zealand White Rabbits according to a previous procedure.⁶ Cells were cultured in Dulbecco's modified Eagle's medium (DMEM; Invitrogen) containing 10% fetal bovine serum (Gibco) and 1% penicillin/streptomycin (Beyotime). Medium was changed every 2 or 3 days. MSCs at passage 2 were used in the following experiments.

Aptamer Binding Assay. Rabbit BMSCs at 70% confluence were washed with warm PBS and incubated with 10nM FAM (5-carboxyfluorescein)-labeled aptamer Apt19s (5'-AGGTCAATGAGGAGGGGACTTAGGACTGGGTT-TATGACCTATGCGTG-FAM-3', synthesized by Sangon Biotech) for 3 hours. Then, the cells were washed twice with PBS and imaged with a fluorescence microscope. The binding efficiency was determined as the percentage of fluorescent cells in 3 randomly selected high-power fields. To verify the specific binding of aptamer to MSCs, rabbit chondrocytes were used as a negative control.

Cell Migration Assay. The ability of aptamer-functionalized SF sponges to recruit MSCs was assessed by cell migration assay in a Transwell model (8 µm; Millipore). Briefly, 10 × 10⁴ MSCs in 100 µL of DMEM were placed in the upper chamber, and the sponge (with or without Apt19s) was put in the lower chamber in the presence of 1-mL DMEM containing 10% fetal bovine serum. After 48 hours, the cells were fixed with 4% paraformaldehyde and stained with crystal violet. The number of cells that migrated to the other side of the membrane was calculated to evaluate the MSC recruitment capacity of Apt19s-functionalized sponge.

Biocompatibility of the Scaffolds. To observe the cell attachment to the scaffold, a slice of scaffold was placed into MSC suspension and cultured at 37°C for 48 hours. Then, the sponge slice was fixed in 2.5% glutaraldehyde and dehydrated with gradient ethanol and acetone. The samples were observed by a ZEISS Crossbeam 340 SEM.

The viability of rabbit BMSCs in SF/HA-Tyr scaffolds was measured with a live/dead cell double-stain kit (Yeasen). In short, MSC-seeded scaffolds were incubated in assay buffer containing 2mM calcein AM and 1.5mM propidium iodine for 30 minutes at 37°C. Labeled cells were visualized with a confocal microscope (Olympus X71). Live cells were stained green, whereas dead cells were stained red.

To measure the cytotoxicity of Apt19s-functionalized SF sponges, extract liquid was first prepared by soaking 50 mg of SF sponge in 10-mL DMEM at 37°C for 24 hours and sterilized with a 0.22-µm filter (Millipore). Then, MSCs were seeded on 96-well plates (5 × 10³ cells/well) 12 hours before the addition of extract liquid (10 µL/100 µL, DMEM). Finally, after 24-, 48-, and 72-hour coculture of sponge extracts with cells, the Cell Counting Kit-8 (Biosharp) was used to evaluate the cytotoxicity. An equal amount of culture medium was used as control.

In Vivo Studies

Implantation of Scaffolds Into Osteochondral Defect in Rabbit Knee Joint. All procedures were in accordance with the *Guide for the Care and Use of Laboratory Animals*

and were approved by the Institutional Animal Care and Use Committee. Twenty-two skeletally mature New Zealand White rabbits were used for the study. Under anesthesia by pentobarbital sodium (50 mg/kg), an osteochondral defect was created with a sterile electric drill (3.2 mm in diameter, 4 mm in depth) in the femoral trochlear groove of the left hindlimb. Visible bleeding was observed to ensure that the defects reached subchondral bone. To examine the MSC recruitment ability of scaffolds (3.2 mm in diameter, 4 mm in height) in vivo, rabbits were implanted with aptamer-functionalized scaffolds ($n = 2$) or scaffolds only ($n = 2$); at 1 and 2 weeks after implantation, the rabbits were sacrificed (1 rabbit each per time point), and the samples were collected for cellularity observation. The other rabbits were randomly divided into 3 groups: nontreated (control group, $n = 6$), aptamer-functionalized scaffolds ($n = 6$), and scaffolds only ($n = 6$). At 6 and 12 weeks postoperatively, 3 rabbits for each group at each time point were euthanized.

Gross and Histologic Evaluation. The degree of cartilage regeneration was evaluated via gross examination. Representative sections of each sample were independently scored by 3 blinded observers (X.W., X.S., T.L.) according to the modified International Cartilage Repair Society (ICRS) gross grading scale (Wayne scoring system).^{22,42}

For histologic analysis, specimens were fixed in 10% formaldehyde, decalcified in EDTA for 3 to 4 weeks, dehydrated in a graded ethanol series, and embedded in paraffin. Samples were cut in the sagittal plane into 4-µm-thick sections through the center of the defect. Paraffin sections were subjected to hematoxylin and eosin staining, safranin O staining, and immunohistochemical staining of collagen types I, II, and X. Sections were analyzed semiquantitatively with the ICRS grade scoring system by 3 blinded observers.^{22,28}

Statistical Analysis

All data were presented as mean ± SD. One-way analysis of variance and Student *t* test were used to calculate the differences among groups. $P < .05$ was considered statistically significant.

RESULTS

Preparation of the Reinforced Sponge/Hydrogel Scaffold

HA-Tyr was synthesized by the coupling reaction of Tyr to the carboxyl groups of HA via EDC/NHS activation (Figure 1B). The structure of the HA-Tyr conjugates was confirmed by ¹H nuclear magnetic resonance (Figure 1C). Except for signals attributable to native HA, new signals at δ 6.69 and δ 6.99 were present in the spectra of HA-Tyr, which were caused by the aromatic protons of Tyr residues. The degree of Tyr molecules per 100 repeating units of HA was about 5.4, calculated by comparing the integrals of the signal at δ 1.84 and the 6.62- to 7.07-ppm region.

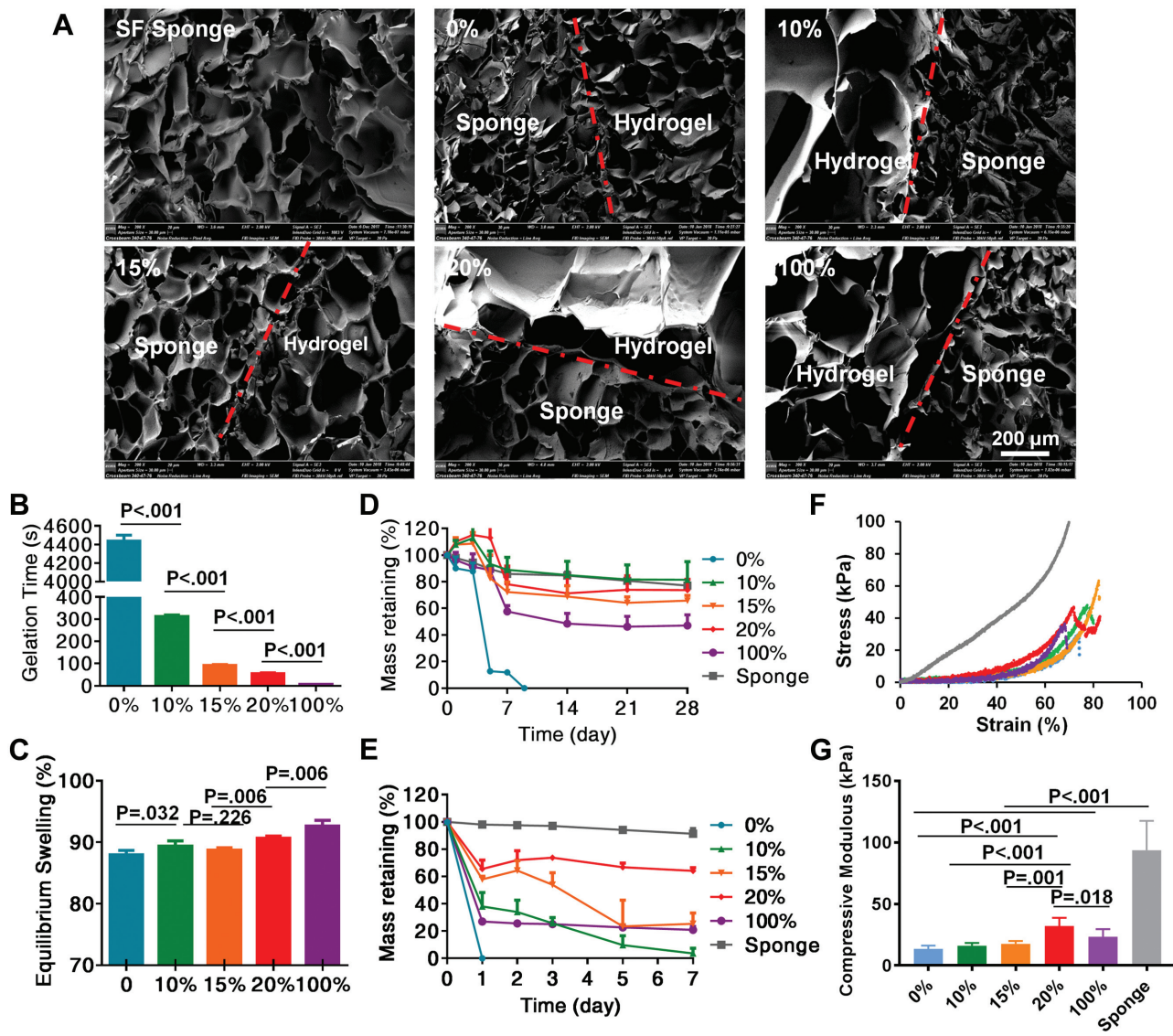


Figure 2. Characterization of the reinforced scaffold. (A) Scanning electron microscope images of the scaffolds; red dotted lines indicate boundaries of hydrogel and sponge. The physicochemical properties of SF/HA-Tyr hydrogels and SF sponge: (B) gelation time, (C) equilibrium swelling ratio, (D) degradation of hydrogel and sponge in phosphate-buffered saline, (E) degradation of hydrogel and sponge in type XIV protease solution, (F) stress-strain curves, and (G) compressive modulus. Mean \pm SD. HA, hyaluronic acid; SF, silk fibroin; Tyr, tyramine.

The gelation mechanism of SF/HA-Tyr is illustrated in Figure 1D, and the macroscopic appearance of the SF/HA-Tyr hydrogel and sponge/hydrogel scaffold is shown in Figure 1E.

Characterization of the Reinforced Scaffold

Morphology. The inner morphology of the scaffolds was determined by cross-sectional SEM images (Figure 2A). The pore size of the SF sponge was around 100 to 200 μm , while hydrogels with different concentrations of HA-Tyr had pore sizes ranging from 100 to 400 μm . Notably, through overnight treatment of infiltration, the SF

sponge was closely integrated with the SF/HA-Tyr hydrogel, ensuring the formation of a reinforced scaffold.

Gelation Time, Swelling Behavior, In Vitro Degradation, and Mechanical Testing. Pure SF solution took >1 hour to reach complete gelation, while pure HA-Tyr reached a gelation state as soon as H_2O_2 and horseradish peroxidase were added. For the SF/HA-Tyr hydrogel, the higher the concentration of HA-Tyr, the quicker the gelation ($P < .001$): the gelation times of the 10%, 15%, and 20% groups were about 5 minutes, 1 minute, and 10 seconds, respectively (Figure 2B).

The SF/HA-Tyr hydrogels had high swelling ratios, ranging from $87.97\% \pm 0.71\%$ to $92.64\% \pm 0.95\%$ (Figure 2C). When the HA-Tyr concentration increased, the

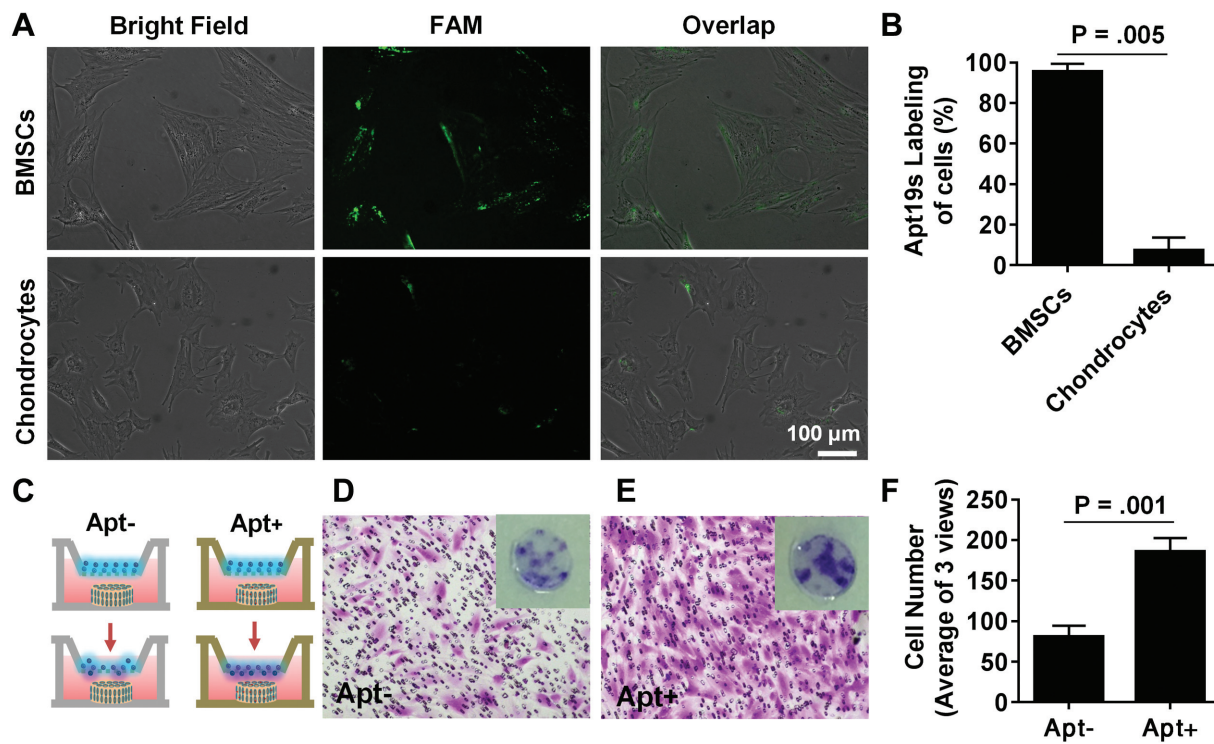


Figure 3. Recruitment of MSCs with Apt19s in vitro. (A) Apt19s binding specificity assay: fluorescent images of the binding of FAM (5-carboxyfluorescein) labeled Apt19s with rabbit bone marrow-derived MSCs (BMSCs) and rabbit chondrocytes. (B) Quantitative data of aptamer binding specificity assay. (C) Schematic diagram of the cell migration assay via the Transwell model. (D) The migrated MSCs toward the aptamer-free (Apt-) sponge were dyed with crystal violet; the insert indicates the overview. (E) The migrated MSCs toward the aptamer-functionalized (Apt+) sponge were dyed with crystal violet; the insert indicates the overview. (F) Quantitative data of MSC migration. Mean \pm SD. MSC, mesenchymal stem cell.

equilibrium swelling was improved, which could be ascribed to the abundant hydrogen bonds in HA-Tyr.

The SF sponge maintained 90% mass in PBS and XIV protease solution, attributing to the formation of β sheet (Figure 2, D and E). The pure SF (0%) and pure HA-Tyr (100%) groups lost weight relatively faster than the composite hydrogel groups. The hydrogels degraded faster in XIV protease solution than in PBS because of the hydrolysis action of XIV protease.

Figure 2F shows the typical stress-strain curves of the SF/HA-Tyr hydrogels and SF sponge. The elastic region of the curves was used to calculate the compressive modulus (Figure 2G). The SF sponge had a significantly higher compressive modulus (93.63 ± 0.24 kPa) than the hydrogels ($P < .001$). Among the hydrogels, 20% concentration of HA-Tyr showed the highest compressive modulus at 32.02 ± 0.07 kPa; therefore, it was used to fabricate the sponge/hydrogel scaffold for in vivo experiments.

Specific Binding and MSC Recruitment of the Aptamer-Functionalized SF Sponge In Vitro. The binding specificity of Apt19s toward MSCs was confirmed by incubating FAM-conjugated Apt19s with rabbit BMSCs and with rabbit chondrocytes as control. After addition of FAM-conjugated Apt19s to culture medium for 3 hours, strong green fluorescence was detected in most MSCs, while hardly any fluorescence was observed in chondrocytes (Figure 3A).

On average of 3 different views, the percentage of FAM-labeled BMSCs was $95.35\% \pm 4.09\%$, while that of FAM-labeled chondrocytes was only $7.26\% \pm 6.31\%$ ($P = .005$) (Figure 3B).

The Transwell system was used to confirm MSC recruitment of Apt19s-functionalized SF sponges in vitro, as illustrated in Figure 3C. Compared with the aptamer-free SF sponge (Figure 3D), the Apt19s-functionalized SF sponge (Figure 3E) attracted more MSCs to migrate to the other side of the membrane. On average of 3 views, there were 185 MSCs migrating toward the Apt19s-functionalized SF sponge but only 80 MSCs to the Apt19s-free SF sponge ($P = .001$) (Figure 3F).

Biocompatibility In Vitro. Figure 4A is a typical SEM image showing cell attachment to the SF sponge. The close-up view (Figure 4B) shows that the cell spreads out on the sponge, with pseudopodia in the cell periphery, indicating a migratory status of the cell. The viability of MSCs in the sponge/hydrogel scaffold is presented in the confocal micrograph (Figure 4C). In 3 dimensions of $800 \times 800 \times 400 \mu\text{m}$, most cells were alive (stained green) and dispersed in this space, while very few cells (stained red) were dead. For cytotoxicity of the Apt19s-functionalized scaffold, the Cell Counting Kit-8 assay result showed that there was no significant difference between the extract liquid group and the culture medium group (Figure 4D).

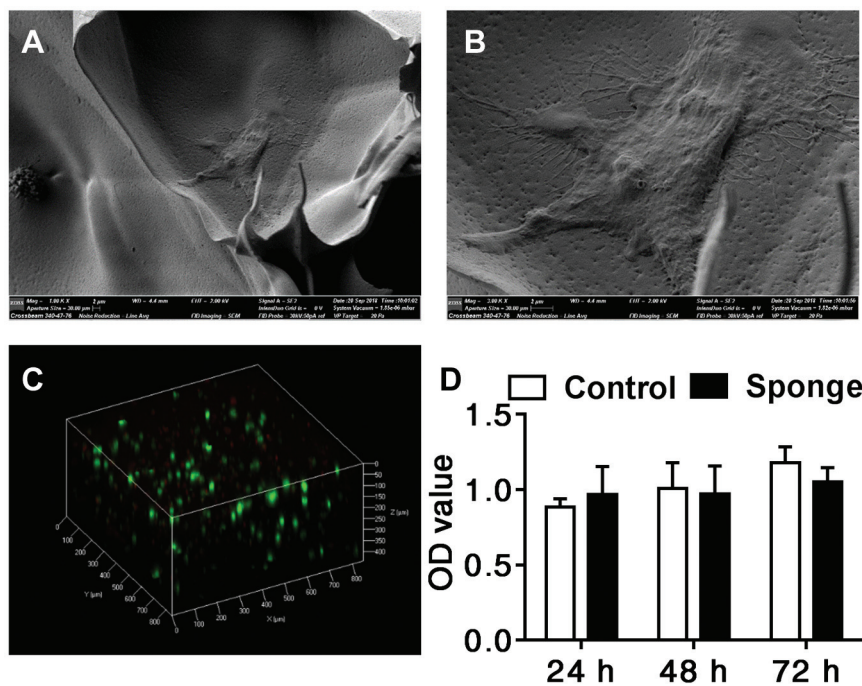


Figure 4. Biocompatibility of the Apt19s-functionalized scaffold. (A) Scanning electron microscope image of a mesenchymal stem cell adhering on the silk fibroin sponge. (B) Enlarged view of the cell in panel A. (C) Confocal image of live and dead cells after 3 days of culture; the scanned area was $800 \times 800 \times 400 \mu\text{m}$. (D) CCK-8 assay measuring cytotoxicity of Apt19s-modified scaffold. Mean \pm SD. OD, optical density.

In Vivo Studies

MSC Recruitment of Aptamer-Functionalized SF Sponge. To further confirm that Apt19s recruited MSCs *in vivo*, Apt19s-functionalized scaffold and scaffold only were implanted into the rabbit osteochondral defects and analyzed for cell numbers within the scaffolds after 1 and 2 weeks (Figure 5A). At 1 week of implantation, hematoxylin and eosin staining of the osteochondral area showed that a large number of cells were located in the aptamer-functionalized scaffold, while there were almost no cells in the aptamer-free scaffold; at 2 weeks of implantation, there were a few cells located in the aptamer-free scaffold, which was still less than the aptamer-functionalized scaffold. Immunohistochemistry results showed that most of the recruited cells were positive in MSC marker CD90/CD105 (Figure 5B).¹⁰

Gross and Histologic Evaluation

Articular joint samples at 6 and 12 weeks after surgery were harvested for gross and histologic evaluation. There was no evident sign of infection or inflammatory response in any of the rabbits. At 6 weeks, the osteochondral defects in the control group were completely covered with newly formed tissue and had a relatively smooth surface, whereas the osteochondral defects in the other 2 groups were partially filled. At 12 weeks, the regenerated tissue in the control group was white, indicating the formation

of fibrous cartilage, whereas the regenerated tissue in the scaffold group was similar to the surrounding normal cartilage in color, indicating the formation of hyaline cartilage-like tissue (Figure 6A). The averaged ICRS score showed similar results to the macroscopic evaluation. The ICRS score was highest in the control group at 6 weeks but highest in the aptamer-functionalized scaffold group at 12 weeks (Figure 6B).

Histologic analysis of osteochondral regeneration was carried out via hematoxylin and eosin staining and safranin O staining. At 6 weeks after implantation, both stainings showed distinct borders between repaired tissue and surrounding tissue, and the neocartilage matrix was shallow as compared with the native matrix in all groups. At 12 weeks, the defects remained concave, although with a smooth surface. The aptamer-functionalized group was better than the other groups in terms of tissue integration and thickness (Figure 6, C and D). Total scores from the ICRS Visual Histologic Assessment Scale were 13, 11.7, and 17 for the control group, scaffold-only group, and aptamer-functionalized scaffold group, respectively (Figure 6E).

Expression of type II, I, and X collagen was qualitatively observed by immunohistochemical staining. For type I collagen (Figure 7A), at 6 weeks all groups showed negative staining; at 12 weeks, there was positive staining at the surface of the regenerated tissue in the control group. For type X collagen (Figure 7B), all groups showed negative staining at 6 and 12 weeks. For type II collagen (Figure 7C), at 6 weeks there was a weak staining in the aptamer-functionalized group; at 12 weeks, the aptamer-functionalized group showed the most

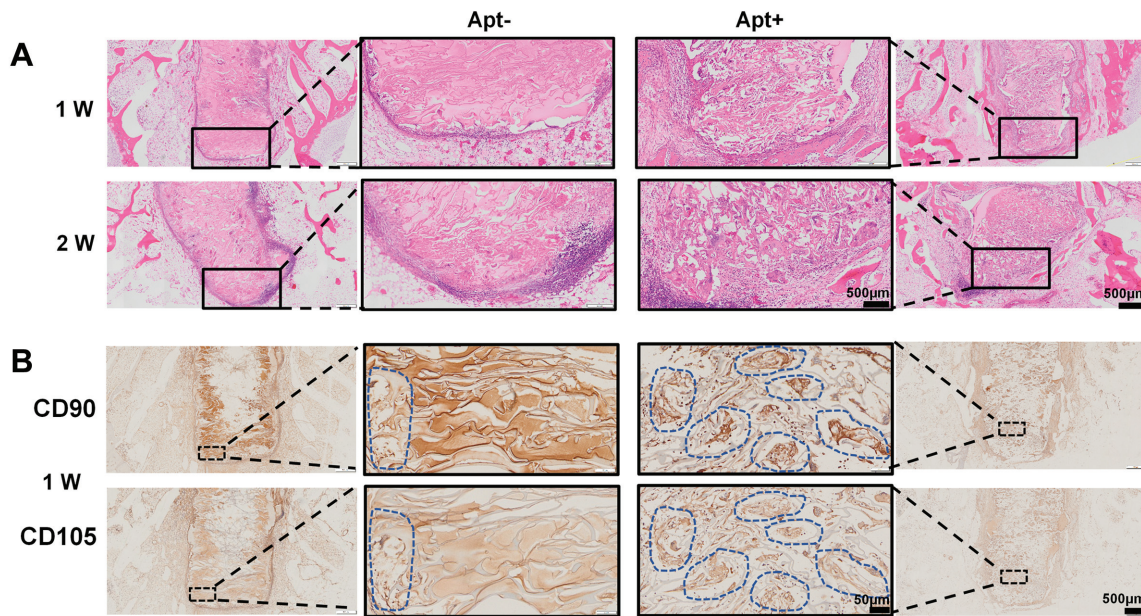


Figure 5. In vivo cell recruitment by aptamer-functionalized scaffold. (A) Representative hematoxylin and eosin staining images of osteochondral region show distinct cellularities between aptamer-functionalized scaffold group (Apt+) and scaffold-only group (Apt-). (B) Immunohistochemistry of mesenchymal stem cell marker CD90/CD105 of the recruited cells. The osteochondral interface is outlined with a rectangle and magnified in close-up views. Blue dotted line indicates cell clusters with positive staining of CD90 or CD105.

deposition and uniform texture, followed by the control group, with the scaffold-only group least.

DISCUSSION

In this study, a “reinforced” scaffold was fabricated by wrapping up an aptamer-functionalized SF sponge with SF/HATyr hydrogel. This scaffold had not only an enhanced mechanical strength in comparison with SF/HATyr hydrogel but also an MSC recruitment capacity both in vitro and in vivo. In the animal model of osteochondral defects, the aptamer-functionalized scaffold achieved a better repair outcome than that of the control group and scaffold-only group.

Articular cartilage has a very limited ability of self-repair, as it contains no nerves, lymphatics, or blood vessels. Moreover, chondrocytes account for only 1% to 5% cartilage volume,³ and their bioactivity could be greatly weakened in cartilage injury or disease. As a result, additional functional cells are usually required for an adequate cartilage repair. Conventionally, chondrocytes or stem cells with chondrogenic potential are injected or implanted into the injury sites. In a “proof of concept” pioneer study, Lee et al²³ used transforming growth factor β3 (TGF-β3)-infused bioscaffolds to fully regenerate the articular surface of the rabbit synovial joint, and they found that TGF-β3 recruited 130% more cells than spontaneous cell migration without TGF-β3, indicating that the cartilage regeneration is probably by homing of endogenous cells. Since then, recruitment of endogenous stem cells to the injury sites has been extensively studied as an alternative

approach for cartilage repair, as it avoids cell isolation, in vitro expansion, and implantation. The most widely used factors so far for recruitment of stem cells for cartilage regeneration are chemokines,^{8,45} growth factors,²⁶ and peptides.^{18,39} As compared with these factors, aptamers have 3 significant advantages^{20,47}: (1) aptamers are much easier to prepare and scale up, (2) aptamers are nonimmunogenic and can be gradually degraded by nucleases and cleared from the blood, and (3) conjugation of aptamers for the attachment of dyes or functional groups is orthogonal and can be readily introduced during synthesis. The aptamer that we used in this study, Apt19s, was first selected by Hou et al¹⁶ through a whole cell systematic evolution of ligands by exponential enrichment to specifically label pluripotent stem cells. For application in cartilage regeneration, both a recent study¹⁷ and our study confirm that Apt19s is very effective in directing the homing of joint-resident MSCs, suggesting that Apt19s is a promising target ligand for endogenous cartilage repair.

We chose SF as the main component of the scaffold because it is Food and Drug Administration approved and has been used in medicine for a variety of applications. SF exhibits in vitro and in vivo biocompatibility, robust mechanical properties, and relatively slow proteolytic biodegradation. In the present study, the SF sponge had a pore size range of 100 to 200 μm with a well-interconnected 3-dimensional porous structure. SF scaffolds with pore sizes of 90 to 250 μm have been shown to provide the best environment for adhesion and proliferation of chondrocytes,¹⁵ and SF scaffolds with pore sizes of 100 to 300 μm have shown better proliferation and extracellular matrix production of

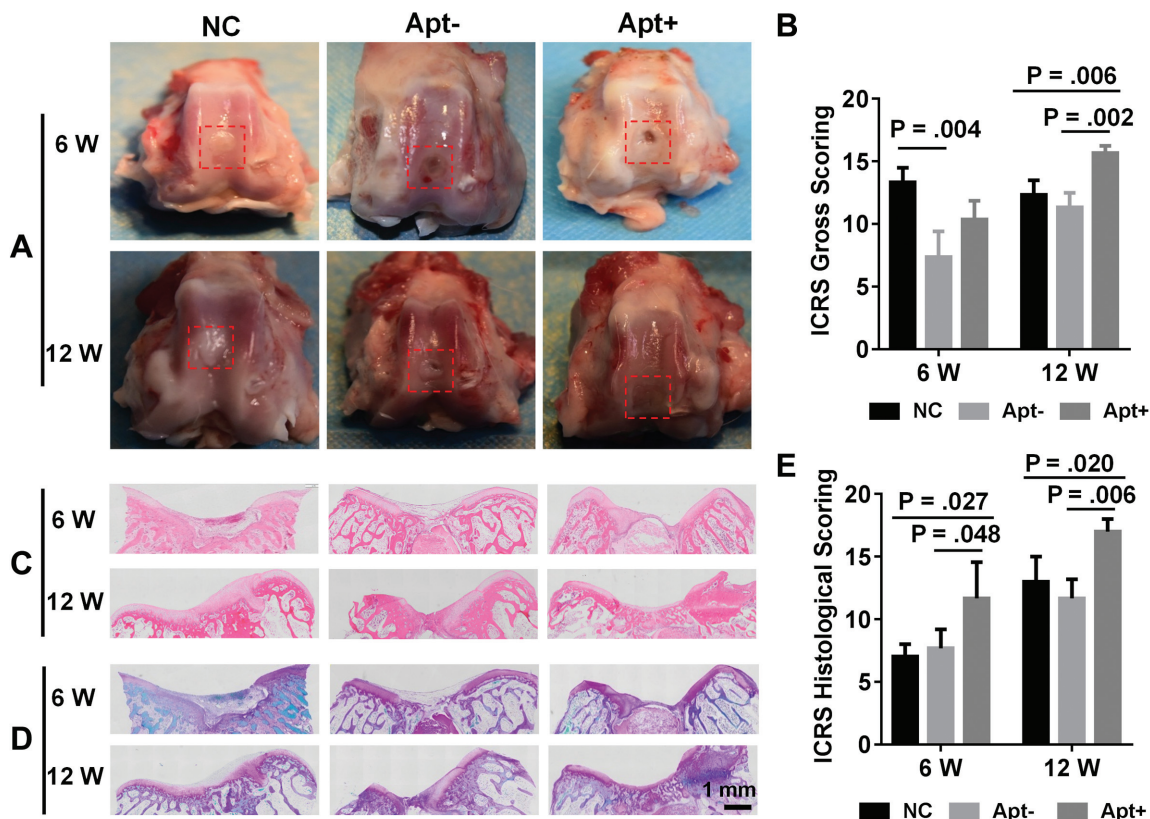


Figure 6. Comparison of cartilage repair in the control group (NC), scaffold-only group (Apt-), and aptamer-functionalized scaffold group (Apt+) at 6 and 12 weeks. (A) Gross appearance of the articular cartilage. Red rectangle indicates the osteochondral defects. (B) Macroscopic analysis for cartilage repair with the modified International Cartilage Repair Society (ICRS) gross grading scale (Wayne scoring system). Histologic analysis for cartilage repair: (C) hematoxylin and eosin staining, (D) safranin O staining, and (E) ICRS visual scoring based on panels C and D. Mean \pm SD.

BMSCs.⁴⁶ Here we demonstrated that our SF sponge, with a similar size range, supported cell anchoring and migration of endogenous MSCs. The degradation rate is another key parameter of scaffolds in cartilage tissue engineering: if a scaffold degrades too fast, it might collapse under continual mechanical loading. In this study, the SF sponge had a relatively slow degradation rate, even in protease XIV solution, possibly because the higher β -sheet content makes the SF sponge more resistant to enzymatic attack.⁴⁴ Note that the SF sponge had a compressive modulus of only 93.63 ± 0.24 kPa, which is lower than that of natural cartilage but still >3 times the modulus of the commercially available type I/III scaffold (25 ± 6 kPa).³³ Besides, the compressive modulus of sponge/hydrogel scaffold would be greatly improved after the SF sponge was infiltrated with SF/HA-Tyr hydrogel. In addition, the SF/HA-Tyr hydrogel could provide (1) a better chondrogenic microenvironment with the cells, as HA is known to promote chondrogenesis and extracellular matrix production,^{21,40} and (2) a mechanical cushion with the scaffold, as the SF/HA-Tyr is overall softer than the embedded SF sponge.

Some observations from the macroscopic and immunohistochemical analyses are worth noting. At 6 weeks after

implantation, the control group actually had the best filling of the osteochondral defects, possibly because of the rabbit's remarkable endogenous healing potential.⁹ At 12 weeks after implantation, the scaffold-only group still had incomplete filling of the defects, indicating that the cells that spontaneously migrated to the scaffold were not sufficient to repair an osteochondral defect of such size. The immunohistochemical analyses at 12 weeks showed that the aptamer-functionalized scaffold group had the best expression of type II collagen, followed by the control group and the scaffold-only group. This indicated the following: (1) as compared with the scaffold-only group, the aptamer-functionalized scaffold group recruited a greater number of cells, and accordingly, there were more cells undergoing chondrogenic differentiation; (2) as compared with the control group, the aptamer-functionalized scaffold group provided a better biomechanical niche for cells to differentiate into hyaline cartilage rather than fibrous cartilage.

This study had some limitations. First, we created osteochondral defects to ensure the homing of bone marrow-derived cells, but we focused only on the results of cell recruitment and cartilage repair, while neglecting the repair of calcified cartilage and subchondral bone.

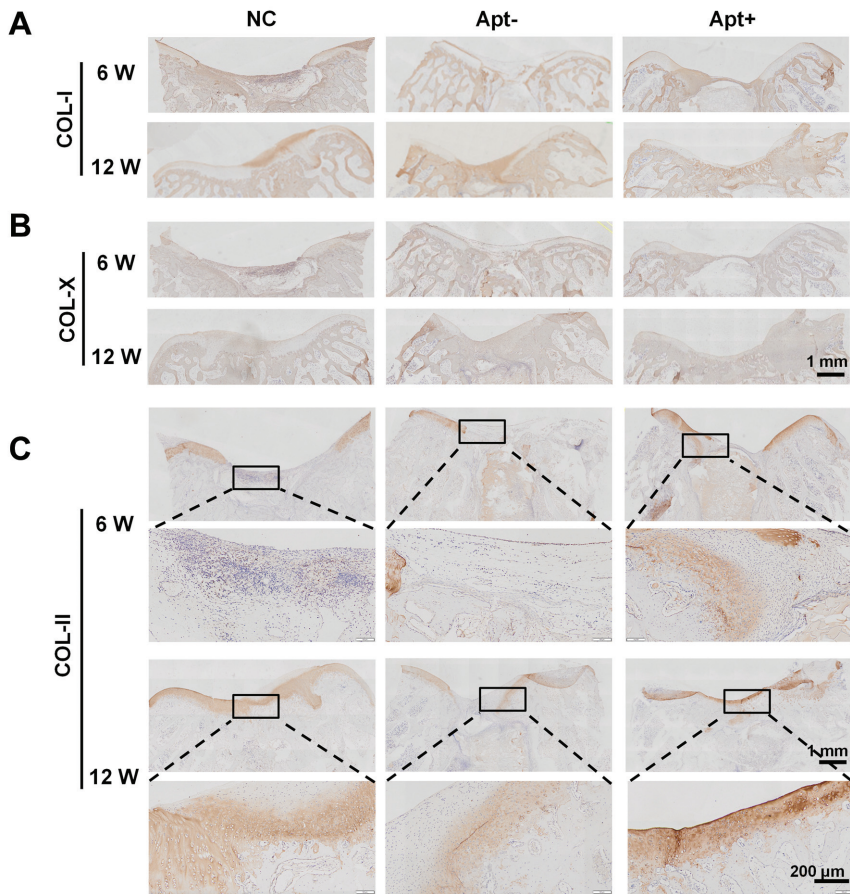


Figure 7. The immunohistochemical staining images for collagen (COL) types (A) I, (B) X, and (C) II of the regenerated tissue at 6 and 12 weeks. COL-II staining in the rectangle area is shown in higher resolution. Apt-, scaffold-only group; Apt+, aptamer-functionalized scaffold group; NC, control group.

Second, the recruited functional cells were probably from the bone marrow, as they were mainly located at the osteochondral interface in the early repair process (1 and 2 weeks). However, we could not rule out the presence of synovium-derived MSCs, since there is strong evidence for the involvement of synovium-derived MSCs in cartilage repair after joint injury.³⁰ The source of the recruited cell needs further investigation.

CONCLUSION

In this study, we developed a reinforced sponge/hydrogel scaffold with clinically available biomaterials: SF and HA. This scaffold was further functionalized with the non-immunogenic aptamer Apt19s to obtain the ability of recruiting endogenous MSCs. Our results demonstrated that the aptamer-functionalized scaffold indeed enhanced endogenous stem cell homing and promoted cartilage repair as compared with the control group and the scaffold-only group. Therefore, this aptamer-functionalized scaffold may offer a tissue-engineering approach for the treatment of osteochondral lesions.

REFERENCES

1. Albright JC, Daoud AK. Microfracture and microfracture plus. *Clin Sports Med.* 2017;36(3):501-507.
2. Baboolal TG, Khalil-Khan A, Theodorides AA, Wall O, Jones E, McGonagle D. A novel arthroscopic technique for intraoperative mobilization of synovial mesenchymal stem cells. *Am J Sports Med.* 2018;46(14):3532-3540.
3. Bhosale AM, Richardson JB. Articular cartilage: structure, injuries and review of management. *Br Med Bull.* 2008;87:77-95.
4. Caldwell KL, Wang J. Cell-based articular cartilage repair: the link between development and regeneration. *Osteoarthritis Cartilage.* 2015;23(3):351-362.
5. Candela ME, Yasuhara R, Iwamoto M, Enomoto-Iwamoto M. Resident mesenchymal progenitors of articular cartilage. *Matrix Biol.* 2014;39:44-49.
6. Cao L, Yang F, Liu G, et al. The promotion of cartilage defect repair using adenovirus mediated Sox9 gene transfer of rabbit bone marrow mesenchymal stem cells. *Biomaterials.* 2011;32(16):3910-3920.
7. Chareancholvanich K, Pornrattanamaneepong C, Narkbunnam R. Increased cartilage volume after injection of hyaluronic acid in osteoarthritis knee patients who underwent high tibial osteotomy. *Knee Surg Sports Traumatol Arthrosc.* 2014;22(6):1415-1423.
8. Chen P, Tao J, Zhu S, et al. Radially oriented collagen scaffold with SDF-1 promotes osteochondral repair by facilitating cell homing. *Biomaterials.* 2015;39:114-123.

9. Chu CR, Szczodry M, Bruno S. Animal models for cartilage regeneration and repair. *Tissue Eng Part B Rev.* 2010;16(1):105-115.
10. Dominici M, Le Blanc K, Mueller I, et al. Minimal criteria for defining multipotent mesenchymal stromal cells: the International Society for Cellular Therapy position statement. *Cytotherapy.* 2006;8(4):315-317.
11. Embree MC, Chen M, Pylawka S, et al. Exploiting endogenous fibrocartilage stem cells to regenerate cartilage and repair joint injury. *Nat Commun.* 2016;7:13073.
12. Fazal N, Latief N. Bombyx mori derived scaffolds and their use in cartilage regeneration: a systematic review. *Osteoarthritis Cartilage.* 2018;26(12):1583-1594.
13. Gao SJ, Wei JC, Lu B, et al. Experimental research on repairing full-thickness articular cartilage defects by transplantation of autologous uncultured bone-marrow-derived mononuclear cells in combination with micro-fracture [in Chinese]. *Zhonghua Yi Xue Za Zhi.* 2012;92(35):2463-2467.
14. Gomoll AH. Microfracture and augments. *J Knee Surg.* 2012;25(1):9-15.
15. Han KS, Song JE, Tripathy N, et al. Effect of pore sizes of silk scaffolds for cartilage tissue engineering. *Macromolecular Research.* 2015;23(12):1091-1097.
16. Hou Z, Meyer S, Propson NE, et al. Characterization and target identification of a DNA aptamer that labels pluripotent stem cells. *Cell Res.* 2015;25(3):390-393.
17. Hu X, Wang Y, Tan Y, et al. A difunctional regeneration scaffold for knee repair based on aptamer-directed cell recruitment. *Adv Mater.* 2017;29(15):1605235.
18. Huang H, Zhang X, Hu X, et al. A functional biphasic biomaterial homing mesenchymal stem cells for in vivo cartilage regeneration. *Biomaterials.* 2014;35(36):9608-9619.
19. Im GI. Endogenous cartilage repair by recruitment of stem cells. *Tissue Eng Part B Rev.* 2016;22(2):160-171.
20. Keefe AD, Pai S, Ellington A. Aptamers as therapeutics. *Nat Rev Drug Discov.* 2010;9(7):537-550.
21. Kim IL, Khetan S, Baker BM, Chen CS, Burdick JA. Fibrous hyaluronic acid hydrogels that direct MSC chondrogenesis through mechanical and adhesive cues. *Biomaterials.* 2013;34(22):5571-5580.
22. Lee BH, Park JN, Lee EJ, Moon YW, Wang JH. Therapeutic efficacy of spherical aggregated human bone marrow-derived mesenchymal stem cells cultured for osteochondral defects of rabbit knee joints. *Am J Sports Med.* 2018;46(9):2242-2252.
23. Lee CH, Cook JL, Mendelson A, Moioli EK, Yao H, Mao JJ. Regeneration of the articular surface of the rabbit synovial joint by cell homing: a proof of concept study. *Lancet.* 2010;376(9739):440-448.
24. Lee F, Chung JE, Kurisawa M. An injectable enzymatically cross-linked hyaluronic acid-tyramine hydrogel system with independent tuning of mechanical strength and gelation rate. *Soft Matter.* 2008;4(4):880-887.
25. Li T, Song X, Weng C, et al. Enzymatically crosslinked and mechanically tunable silk fibroin/pullulan hydrogels for mesenchymal stem cells delivery. *Int J Biol Macromol.* 2018;115:300-307.
26. Luo Z, Jiang L, Xu Y, et al. Mechano growth factor (MGF) and transforming growth factor (TGF)-beta3 functionalized silk scaffolds enhance articular hyaline cartilage regeneration in rabbit model. *Biomaterials.* 2015;52:463-475.
27. Ma B, Leijten JC, Wu L, et al. Gene expression profiling of dedifferentiated human articular chondrocytes in monolayer culture. *Osteoarthritis Cartilage.* 2013;21(4):599-603.
28. Mainil-Varlet P, Aigner T, Brittberg M, et al. Histological assessment of cartilage repair: a report by the Histology Endpoint Committee of the International Cartilage Repair Society (ICRS). *J Bone Joint Surg Am.* 2003;85(suppl 2):45-57.
29. Makris EA, Gomoll AH, Malizos KN, Hu JC, Athanasiou KA. Repair and tissue engineering techniques for articular cartilage. *Nat Rev Rheumatol.* 2015;11(1):21-34.
30. McGonagle D, Baboolal TG, Jones E. Native joint-resident mesenchymal stem cells for cartilage repair in osteoarthritis. *Nat Rev Rheumatol.* 2017;13(12):719-730.
31. Moran CJ, Pascual-Garrido C, Chubinskaya S, et al. Restoration of articular cartilage. *J Bone Joint Surg Am.* 2014;96(4):336-344.
32. Mueller MB, Tuan RS. Functional characterization of hypertrophy in chondrogenesis of human mesenchymal stem cells. *Arthritis Rheum.* 2008;58(5):1377-1388.
33. Nurnberger S, Schneider C, van Osch GVM, et al. Repopulation of an auricular cartilage scaffold, AuriScaff, perforated with an enzyme combination. *Acta Biomater.* 2019;86:207-222.
34. Pelttari K, Winter A, Steck E, et al. Premature induction of hypertrophy during in vitro chondrogenesis of human mesenchymal stem cells correlates with calcification and vascular invasion after ectopic transplantation in SCID mice. *Arthritis Rheum.* 2006;54(10):3254-3266.
35. Schulze-Tanzil G. Activation and dedifferentiation of chondrocytes: implications in cartilage injury and repair. *Ann Anat.* 2009;191(4):325-338.
36. Solheim E, Hegna J, Inderhaug E, Oyen J, Harlem T, Strand T. Results at 10-14 years after microfracture treatment of articular cartilage defects in the knee. *Knee Surg Sports Traumatol Arthrosc.* 2016;24(5):1587-1593.
37. Solheim E, Hegna J, Strand T, Harlem T, Inderhaug E. Randomized study of long-term (15-17 years) outcome after microfracture versus mosaicplasty in knee articular cartilage defects. *Am J Sports Med.* 2018;46(4):826-831.
38. Sophia Fox AJ, Bedi A, Rodeo SA. The basic science of articular cartilage: structure, composition, and function. *Sports Health.* 2009;1(6):461-468.
39. Sun X, Yin H, Wang Y, et al. In situ articular cartilage regeneration through endogenous reparative cell homing using a functional bone marrow-specific scaffolding system. *ACS Appl Mater Interfaces.* 2018;10(45):38715-38728.
40. Toh WS, Lim TC, Kurisawa M, Spector M. Modulation of mesenchymal stem cell chondrogenesis in a tunable hyaluronic acid hydrogel microenvironment. *Biomaterials.* 2012;33(15):3835-3845.
41. Wang Y, Blasioli DJ, Kim HJ, Kim HS, Kaplan DL. Cartilage tissue engineering with silk scaffolds and human articular chondrocytes. *Biomaterials.* 2006;27(25):4434-4442.
42. Wayne JS, McDowell CL, Shields KJ, Tuan RS. In vivo response of poly(lactic acid-alginate) scaffolds and bone marrow-derived cells for cartilage tissue engineering. *Tissue Eng.* 2005;11(5-6):953-963.
43. Yodmuang S, McNamara SL, Nover AB, et al. Silk microfiber-reinforced silk hydrogel composites for functional cartilage tissue repair. *Acta Biomater.* 2015;11:27-36.
44. You R, Xu Y, Liu Y, Li X, Li M. Comparison of the in vitro and in vivo degradations of silk fibroin scaffolds from mulberry and nonmulberry silkworms. *Biomed Mater.* 2014;10(1):015003.
45. Yu Y, Brouillette MJ, Seol D, Zheng H, Buckwalter JA, Martin JA. Use of recombinant human stromal cell-derived factor 1alpha-loaded fibrin/hyaluronic acid hydrogel networks to achieve functional repair of full-thickness bovine articular cartilage via homing of chondrogenic progenitor cells. *Arthritis Rheumatol.* 2015;67(5):1274-1285.
46. Zhang Y, Fan W, Ma Z, et al. The effects of pore architecture in silk fibroin scaffolds on the growth and differentiation of mesenchymal stem cells expressing BMP7. *Acta Biomater.* 2010;6(8):3021-3028.
47. Zhou J, Rossi J. Aptamers as targeted therapeutics: current potential and challenges. *Nat Rev Drug Discov.* 2017;16(3):181-202.
48. Zhu G, Chen X. Aptamer-based targeted therapy. *Adv Drug Deliv Rev.* 2018;134:65-78.